

Photon-density wave correlation spectroscopy detects large-scale fluctuations in turbid media

V. Toronov,* M. Filiaci, S. Fantini, and E. Gratton

*Laboratory for Fluorescence Dynamics, Department of Physics, University of Illinois at Urbana-Champaign,
1110 West Green Street, Urbana, Illinois 61801-3080*

(Received 10 December 1997)

We study the fluctuations in the photon-density wave parameters [average intensity (dc), modulation amplitude, and phase] caused by macroscopic fluctuations in the optical properties of turbid media. We present both a theoretical analysis based on diffusion theory and its experimental verification on a strongly scattering suspension containing absorbing particles (1–1.6 mm effective diameter) in turbulent motion. The photon-density waves are induced by the laser diode output (750 nm), which is intensity-modulated at 110 MHz. The dc, amplitude, and phase are acquired with an acquisition time per data point of 8 ms, which corresponds to a frequency bandwidth of 62.5 Hz. We have found that in the presence of the absorbing particles, the dc and phase average values and power spectra are in good agreement with our theoretical predictions. We have verified that our instrument can extend the measured frequency band up to the kHz region, which is appropriate for the study of fluctuations of optical parameters in biological tissues. [S1063-651X(98)01708-5]

PACS number(s): 87.64.Ni, 42.25.Gy, 41.20.Jb, 42.62.Be

I. INTRODUCTION

In recent years the correlation spectroscopy technique was used to study optically thick media that exhibit a high degree of multiple scattering [1–4]. This technique, called diffusing wave spectroscopy (DWS), relates scattered light fluctuations to the motion of scattering particles. DWS was proposed as a tool for the study of microscopical particle motion (over a fraction of the optical wavelength) in multiply scattering media such as colloids and microemulsions.

Biological tissues typically display strong light scattering, and therefore can be important subjects for DWS applications. However, in addition to the small-scale fluctuations due to the motion of the microscopical scatterers, biological activity in tissues may produce large-scale spatial and temporal fluctuations of tissue optical properties in the near-infrared band. It was demonstrated that such fluctuations in the brain may result, for example, from hemodynamics [5,6] and neuronal activity [7]. In particular, it was found that visual stimulation induces local changes in the optical properties of the human brain visual area [7]. It was also noted that near-infrared tissue spectroscopy has an advantage over other techniques for studying neuronal processes in that it potentially combines good temporal resolution (10–50 ms) with a spatial resolution of the order of 5 mm [5,7]. Therefore, the analysis of large-scale fluctuations in near-infrared photon migration may provide a useful tool for the study of functional processes.

In this paper we present a theoretical and experimental study of a system exhibiting large-scale (\sim mm) optical parameter fluctuations. The idea is to induce photon-density waves in a turbid medium using an intensity-modulated light source. The phase velocity and the attenuation of these photon density waves depend on optical properties of the medium and on the modulation frequency [8–11]. The localized areas having optical properties differing from those of the

background medium affect the photon-density waves by absorption and refraction processes. Similarly to the DWS method, we relate the fluctuations in the photon-density wave parameters to the optical fluctuations in turbid media. The differences from DWS are that (i) in our case the measurable parameters are the average intensity (dc), the modulation amplitude (ac), and the phase (Φ) of the photon density wave (having a frequency of \sim 100 MHz), while in DWS the only measurable value is the light intensity, and (ii) in our case the process under study is the large-scale (\sim mm) local optical property change, while in DWS it is the microscopic particle displacement (\sim nm).

The purpose of our investigation is to show the potential of this approach for *in vivo* studies of biological systems, and to determine the instrumental capabilities. The experimental part of our work is based on frequency-domain measurements of the diffuse photon-density wave propagating in a Liposyn suspension with fluctuating optical properties. The spatial and temporal fluctuations of the scattering and absorption coefficients are caused by the motion of absorbing particles having a size of 1.0–1.6 mm. The frequency-domain parameters analyzed in this study are the dc and phase of the photon-density wave. Similarly to the standard DWS approach, we use the diffusion approximation of light transport in a turbid medium [8–11] to express the statistical characteristics of frequency domain parameters (average values and autocorrelation functions) in terms of those of the particle motion.

The paper is organized as follows. In Sec. II we describe our experimental apparatus and methods. In Sec. III we derive the expressions for the mean values and autocorrelation functions of the frequency-domain parameters based on a simplified statistical model for the motion of the absorbing particles. In Sec. IV we compare the experimental measurements with the theoretical predictions. The discussion of the results is presented in Sec. V.

II. EXPERIMENTAL SETUP AND METHOD

The central part of our experimental setup (Fig. 1) consists of a container (a 1-L beaker) filled with an aqueous

*FAX: (217) 244-7187.

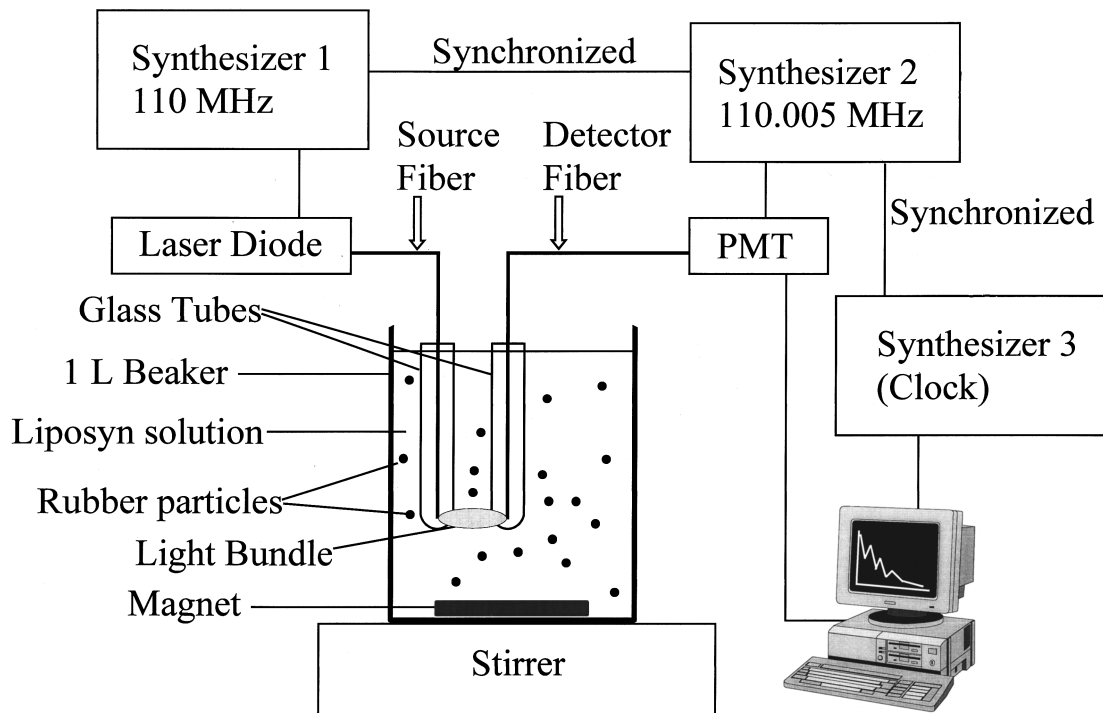


FIG. 1. Schematic of the experimental setup, PMT is the photomultiplier tube. The Synthesizer 3 is used as a clock for the sampling synchronization.

Liposyn suspension (Abbott Laboratories), in which small black rubber particles undergo turbulent motion caused by a magnetic-stick stirrer. The average velocity of particle motion is controlled by adjustment of the stirrer rotation frequency. In each experiment we use particles of approximately equal size, either 1 mm or 1.6 mm effective diameter.

The 750 nm light emitted by the laser diode (~ 2 mW average power, Sharp LT030MD) is guided to the medium through a multimode silica optical fiber (source fiber) having a core diameter of $600 \mu\text{m}$ and a numerical aperture of 0.39 (Thorlabs, FT-600-EMT). A glass fiber bundle (detector fiber, internal diameter: 3.2 mm, numerical aperture: 0.56, Oriel, Model No. 77527) collects the scattered light and conducts it to the photomultiplier tube (PMT, Hamamatsu

R928). To prevent significant light blockage by particles coming very close to the fiber ends, both fibers are placed in glass tubes such that the ends are approximately in the center of the hemisphere at the bottom of the tubes, which have a diameter of 1.3 cm. The tubes are filled with the same medium as the entire container. The distance between the source and detector fibers ranges from 1.4 to 2.4 cm, which corresponds to a minimum distance between the tube walls ranging from 0.1 to 1.1 cm.

The laser current and the PMT voltage are modulated by the synchronized synthesizers at 110 and 110.005 MHz respectively. The signal from the PMT at the difference frequency (also called the cross-correlation frequency) is applied to the input of an interface card (ISS A2D, ISS Inc., Champaign, IL) for an IBM-PC computer, where the data processing is performed to obtain dc, ac, and Φ [12]. Figure 2 shows a sample of the dc and phase temporal evolution obtained with an acquisition time of 8 ms. The left part of the

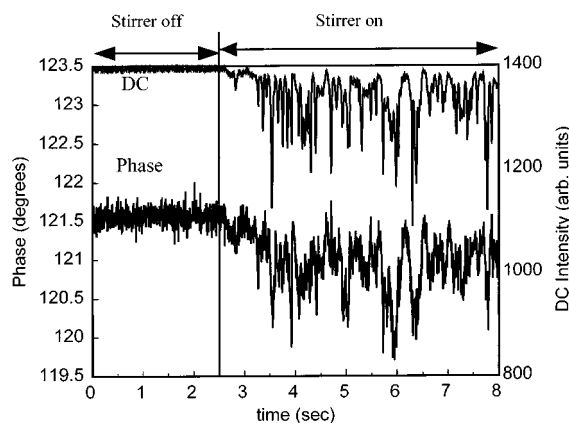


FIG. 2. Time traces of the dc and phase signals before and after the stirrer is turned on. The average particle radius is 0.79 mm; the particle concentration is 0.3 cm^{-3} ; the magnet rotation frequency is about 2.5 Hz; the acquisition time is 8 ms per data point.

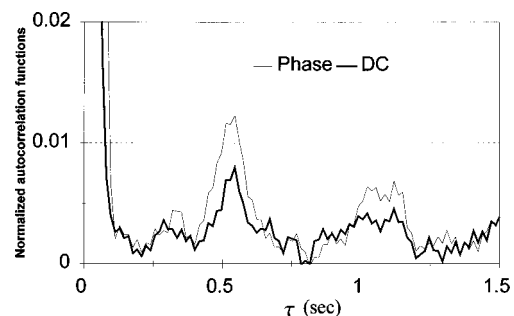


FIG. 3. Phase and dc normalized autocorrelation functions obtained from the experimental power spectra using the discrete inverse Fourier transform. Experimental conditions are the same as in Fig. 2, and the total time per sweep is 8 sec.

TABLE I. Results of the least χ^2 fit of the average phase and dc change in three different experiments. Numbers in parentheses are the standard deviation errors in the last digits.

Data set	Average change in	Parameter	Expected	Fitted	χ^2	Fig. No.
1	dc for different concentrations of large particles	a (mm)	0.79(1)	0.68(2)	1.1	
		n_1 (cm^{-3})	0.3	0.29(4)		
		n_2 (cm^{-3})	0.4	0.42(5)		
		n_3 (cm^{-3})	0.5	0.49(5)		
		n_4 (cm^{-3})	0.6	0.61(5)		
	phase for different concentrations of large particles	a (mm)	0.79(1)	0.66(1)	1.4	5(a)
		n_1 (cm^{-3})	0.3	0.32(5)		
		n_2 (cm^{-3})	0.4	0.40(5)		
		n_3 (cm^{-3})	0.5	0.47(5)		
		n_4 (cm^{-3})	0.6	0.54(5)		
2	dc for different concentrations of small particles	a (mm)	0.50(1)	0.38(1)	1.8	5(b)
		n_1 (cm^{-3})	0.4	0.3(1)		
		n_2 (cm^{-3})	0.8	0.8(1)		
		n_3 (cm^{-3})	1.2	1.3(1)		
		n_4 (cm^{-3})	1.6	1.7(1)		
		n_5 (cm^{-3})	2.0	2.0(1)		
	phase for different concentrations of small particles	a (mm)	0.50(1)	0.35(1)	1.5	
		n_1 (cm^{-3})	0.4	0.2(2)		
		n_2 (cm^{-3})	0.8	0.8(1)		
		n_3 (cm^{-3})	1.2	1.2(1)		
3	phase for different μ_a values (small particles)	a (mm)	0.50(1)	0.50(1)	1.7	5(c)
		μ_{a1} (cm^{-1})	0.044(2)	0.041(2)		
		μ_{a2} (cm^{-1})	0.057(2)	0.050(2)		
		μ_{a3} (cm^{-1})	0.073(2)	0.059(1)		
		μ_{a4} (cm^{-1})	0.088(2)	0.077(3)		

plot corresponds to the situation when the mixer is off, so that the particles rest on the bottom of the beaker, and the right part (after $t \approx 2.5$ s) corresponds to the fluctuation regime, when the stirrer is on. One can see that when the mixer is on, both the phase and the dc exhibit fluctuations over some average value, which is different from that when the mixer is off. The time series of the dc and phase values were further processed to obtain the time-averaged values of the frequency domain parameters and their fluctuation power spectra. For the power spectrum analysis two characteristics of the data acquisition are important, namely the sampling rate (which is inverse of the acquisition time) and the total length of the time sweep. The upper limit of the sampling rate is determined by the cross-correlation frequency (5 kHz for our instrument) and is the higher the larger the frequency is. This is because the frequency-domain parameter evaluation employs the fast Fourier transform of a cross-correlation waveform, in general obtained by averaging over a number of acquired waveforms [12]. For the measurements reported in this work, the acquisition time per point was 8 ms, which corresponds to 40 periods of the cross-correlation wave. All results were verified to be in good quantitative agreement

with those obtained at different acquisition times from 4 to 16 ms per point. An acquisition time of 4 (16) ms corresponds to a frequency bandwidth of 125 (31.25) Hz in the power spectrum. The total time of a sweep is restricted only by the capacity of the computer memory. In our measurements it was 8.2 s, which corresponds to a frequency reso-

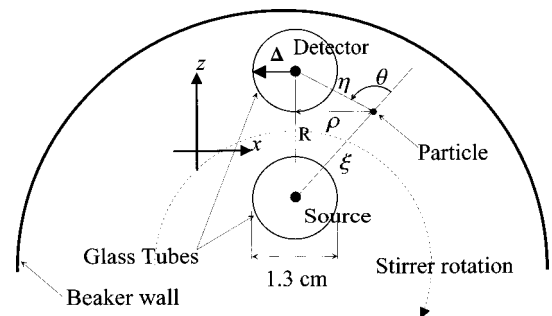


FIG. 4. View of the beaker setup from above. Coordinate axes x and z show only the spatial directions and are not attached to any fixed Cartesian coordinate system. The vertical y axis is perpendicular to the plane of the figure.

lution of 0.125 Hz. Figure 3 shows typical dc and phase normalized autocorrelation functions (autocorrelation functions normalized to unity at zero time) obtained from the experimentally acquired power spectra by means of the inverse discrete Fourier transform.

Our technique also allows us to obtain the absorption and reduced scattering coefficients of the medium from the plots of the dc and phase vs source-detector distance in the absence of particles. The details on the corresponding technique may be found in [13,14]. In all the measurements reported here the reduced scattering coefficient μ'_s of the Lyposin suspension was $9.8 \pm 0.1 \text{ cm}^{-1}$. The absorption coefficient μ_a was always $0.042 \pm 0.001 \text{ cm}^{-1}$, apart from the experiment where we varied μ_a (data set 3 in Table I).

III. THEORY

A. The model

Figure 4 shows a close up view of the beaker setup and explains the geometry-related notations used below.

We describe the signal fluctuations due to the particle motion using the diffusion approximation to the theory of light propagation in turbid media [8–11]. In this approximation the light energy density as a function of time and space coordinates (the so-called ‘‘photon density’’) obeys the general diffusion equation and the particular boundary conditions specified by the light absorption and scattering at the boundaries. We assume that the rubber particles contribute to the signal change by absorbing photons from all possible paths passing through a given particle. Since the particles used in the experiment are small, one can neglect the contributions from those photon paths that include more than one particle. In this approximation the solution to the diffusion equation may be written as

$$G = U + \sum_{j=1}^{N_p} \delta u_j, \quad (1)$$

where $U = U_{\text{dc}} + U_{\text{ac}}$ is the sum of dc and ac photon densities created by the light source in the absence of particles, $\delta u_j = \delta u_{\text{dc}}(\mathbf{r}_j) + \delta u_{\text{ac}}(\mathbf{r}_j, \omega)$ is the sum of dc and ac contributions from the particle having coordinate \mathbf{r}_j , and N_p is the total number of particles in the beaker. The simplest analytical form of δu_j is that for a spherical particle at position \mathbf{r} , for which it may be expressed as the sum of the dc and ac terms both having the form

$$\begin{aligned} \delta u(\mathbf{r}, \omega) = S(\omega) \frac{3\mu'_s}{v} \sum_{l=0}^{\infty} A_{\omega l} h_l^{(1)}(k_{\omega} \xi) h_l^{(1)}(k_{\omega} \eta) \\ \times (k_{\omega} \eta) Y_{l,0}(\theta, 0) e^{-i\omega t}, \end{aligned} \quad (2)$$

where ξ and η are the distances from the particle to the source and the detector, respectively (see Fig. 4). Note that as a result of the cylindrical symmetry with respect to the z axis passing through the source and detector (Fig. 4), ξ and η are the only independent coordinates entering Eq. (2), since the angle θ may be expressed in their terms. In Eq. (2), $h_l^{(1)}(x)$ are the spherical Hankel functions of the first kind, $Y_{l,m}(\theta, \phi)$ are spherical harmonics, $A_{\omega l}$ are the numerical

constants defined by the boundary conditions [15], v is the speed of light in the medium, and $S(\omega)$ is the source power at angular frequency ω (for the dc, $\omega=0$). In Eq. (2), k_{ω} is the diffusion wave number,

$$\begin{aligned} k_{\omega} = \sqrt{\frac{3}{2} \mu_a \mu'_s} \left[\left(-1 + \sqrt{1 + \frac{\omega^2}{c^2 \mu_a^2}} \right)^{1/2} \right. \\ \left. + i \left(1 + \sqrt{1 + \frac{\omega^2}{c^2 \mu_a^2}} \right)^{1/2} \right], \end{aligned} \quad (3)$$

where μ_a and μ'_s are, respectively, the absorption and the reduced scattering coefficients of the medium.

The constants $A_{\omega l}$ in Eq. (2) depend on the size of the object and on its scattering and absorbing properties [15]. Using the expressions for $A_{\omega l}$ derived in [15] one can check that for perfectly absorbing objects having a diameter smaller than about 5 mm, the magnitudes of $A_{\omega l}$ monotonically decrease by several orders of magnitude for each successive l . Keeping only the zero-order term we have

$$\delta u(\mathbf{r}, \omega) = S(\omega) A_{\omega} \frac{3\mu'_s}{v} \frac{e^{ik_{\omega}(\xi+\eta)}}{4\pi\xi\eta}, \quad (4)$$

where

$$A_{\omega} = i \frac{e^{-ik_{\omega}a}}{k_{\omega}} \frac{2k_{\omega}a \cos(k_{\omega}a) - (2 + 3\mu'_s a) \sin(k_{\omega}a)}{2k_{\omega}a + i(2 + 3\mu'_s a)}. \quad (5)$$

In Eq. (5), a is the radius of the spherical object. Note that if one takes typical values for near-infrared μ_a and μ'_s in biological tissues (e.g., $\mu_a = 0.1 \text{ cm}^{-1}$, $\mu'_s = 8 \text{ cm}^{-1}$), where $k_{\omega} \approx 1 \text{ cm}^{-1}$, and since $a \ll 1 \text{ cm}$, we can set $\cos(k_{\omega}a) = 1$ and $\sin(k_{\omega}a) = k_{\omega}a$, so we obtain the approximation

$$A_{\omega} \approx - \frac{3\mu'_s a^2}{2 + 3a\mu'_s}. \quad (6)$$

This is unlike the case of a nonperfect absorber, for which the zero-order term in Eq. (2) is proportional to a^3 . Note that the modulation frequency ω does not enter Eq. (6), so that in this approximation the coefficients A_{ω} for the dc and ac parts of the signal are equal.

B. Average values of dc and phase fluctuations

If one considers a homogeneous spatial distribution of absorbing particles, and by assuming that all particles are spheres of the same radius a , the ensemble average of the dc fluctuation $\langle \delta U_{\text{dc}} \rangle = \langle \sum_j \delta u(\mathbf{r}_j), 0 \rangle$ is given by the volume integral of the right-hand side of Eq. (4) at $\omega=0$, multiplied by the particle concentration n . Taking into account that in terms of the variables ξ and η the volume element is $(2\pi\xi\eta/R)d\xi d\eta$ (where R is the source-detector separation), and that the source and the detector are protected from the particles by tubes of radius Δ , one obtains for the average dc change the expression

$$\langle \delta U_{\text{dc}} \rangle = S(0) \frac{3\mu'_s A_0 n}{v} \frac{\alpha(R-2\Delta) + 1 - e^{-2\alpha\Delta}}{2R \alpha^2} e^{-\alpha R}, \quad (7)$$

where $\alpha = \sqrt{3\mu_a\mu'_s}$, or using the approximations in Eq. (6),

$$\langle \delta U_{\text{dc}} \rangle \approx -S(0) \frac{(3\mu'_s)^2 a^2 n e^{-\alpha R}}{2 + 3a\mu'_s} \frac{\alpha(R-2\Delta) + 1 - e^{-2\alpha\Delta}}{2vR \alpha^2}. \quad (8)$$

For comparison with the experimental measurements it is more convenient to use the relative average dc fluctuation $\langle \delta U_{\text{dc}} \rangle / U_{\text{dc}}$. Assuming an infinite medium, for which $U_{\text{dc}} = S(0)(3\mu'_s e^{-\alpha R} / 4\pi v R)$, one gets

$$\frac{\langle \delta U_{\text{dc}} \rangle}{U_{\text{dc}}} = \frac{-6\pi n \mu'_s a^2}{2 + 3a\mu'_s} \frac{\alpha(R-2\Delta) + 1 - e^{-2\alpha\Delta}}{\alpha^2}. \quad (9)$$

Note that the right-hand side of Eq. (9) is a linear function of R .

To estimate the average phase fluctuation we write the ac part of the signal in the form

$$S(\omega) \frac{e^{ik\omega R - i\omega t}}{4\pi v R} \left(1 - A_\omega R \sum_j \frac{e^{ik\omega(\xi_j + \eta_j - R)}}{\xi_j \eta_j} \right), \quad (10)$$

where the factored term is the ac signal with no particles. It follows from Eq. (10) that the tangent of the phase change $\delta\Phi$ due to the particles is

$$\tan(\delta\Phi) = \frac{R \operatorname{Im} \left(A_\omega \sum_j \frac{e^{ik(\xi_j + \eta_j - R)}}{\xi_j \eta_j} \right)}{1 - R \operatorname{Re} \left(A_\omega \sum_j \frac{e^{ik(\xi_j + \eta_j - R)}}{\xi_j \eta_j} \right)}. \quad (11)$$

Note that for particles less than a few millimeters in diameter the absolute value of A_ω is much smaller than R . Let us also take into account the fact that the values of ξ_j and η_j in Eq. (10) are of the order of $R/2$ and greater than 0.65 cm (the test tube radius). For this reason the second term in the denominator of Eq. (11) may be neglected. This is valid for particles of small enough size if their concentration is not too large. Since in our measurements the instantaneous phase deviation values from the value in the absence of particles lie within a few degrees (see Fig. 2), one can also replace $\tan(\delta\Phi)$ by $\delta\Phi$, so that finally the phase fluctuation may be expressed as the sum over the single-particle contributions $\delta\phi(\mathbf{r}_j)$ as

$$\delta\Phi \approx \sum_j \delta\phi(\mathbf{r}_j), \quad (12)$$

where

$$\delta\phi(\mathbf{r}_j) = R \operatorname{Im} \left(A_\omega \frac{e^{ik\omega(\xi_j + \eta_j - R)}}{\xi_j \eta_j} \right). \quad (13)$$

This approximation leads to the expression for the average phase fluctuation:

$$\begin{aligned} \langle \delta\Phi \rangle &\approx R n \operatorname{Im} \left(A_\omega \int \frac{e^{ik\omega(\xi + \eta - R)}}{4\pi \xi \eta} dV \right) \\ &= 2\pi n \operatorname{Im} \left(\frac{A_\omega}{k^2} [-1 + e^{2ik\Delta} + ik(R-2\Delta)] \right), \end{aligned} \quad (14)$$

from which one can see that $\langle \delta\Phi \rangle$ is a linear function of the source-detector distance R . Using the approximation (6) for A_ω , Eq. (14) becomes

$$\langle \delta\Phi \rangle \approx -\frac{6\pi n \mu'_s a^2}{2 + 3a\mu'_s} \operatorname{Im} \left(\frac{-1 + e^{2ik\Delta} + ik(R-2\Delta)}{k^2} \right). \quad (15)$$

C. Autocorrelation functions

If one assumes a homogeneous particle distribution in the medium and the independence of the motion of each particle from the others, the dc autocorrelation function $K_{\text{dc}}(\tau)$ may be given by the expression [16]

$$K_{\text{dc}}(\tau) = n \int \int \delta u(\mathbf{r}_1, 0) \delta u(\mathbf{r}_2, 0) W_\tau(\mathbf{r}_1 \rightarrow \mathbf{r}_2) d^3\mathbf{r}_1 d^3\mathbf{r}_2, \quad (16)$$

where $\delta u(\mathbf{r}, 0)$ is the single-particle contribution to the dc change given by Eq. (4), \mathbf{r}_1 and \mathbf{r}_2 are the coordinates of a particle at time moments t and $t + \tau$, respectively, $W_\tau(\mathbf{r}_1 \rightarrow \mathbf{r}_2)$ is the probability density for the particle displacement from point \mathbf{r}_1 at time t to point \mathbf{r}_2 at time $t + \tau$, and n is the concentration of particles. The particular form of $W_\tau(\mathbf{r}_1 \rightarrow \mathbf{r}_2)$ is determined by the nature of the particle motion and is not known for the given environment. We assume that the vector of a particle displacement $\mathbf{r}_2 - \mathbf{r}_1$ may be represented as a sum of the regular periodical component $\mathbf{r}'(\tau)$ describing the rotation in the horizontal plane around the beaker vertical axis, and a random component \mathbf{r}'' . For this model the probability density may be written as [17]

$$W_\tau(\mathbf{r}_1 \rightarrow \mathbf{r}_2) = \frac{(4\pi\tau)^{-3/2}}{\sqrt{D_x D_y D_z}} \exp \left(-\frac{(x'')^2}{4D_x\tau} - \frac{(y'')^2}{4D_y\tau} - \frac{(z'')^2}{4D_z\tau} \right), \quad (17)$$

and the integration over \mathbf{r}_2 in Eq. (16) reduces to that over \mathbf{r}'' . Since the detector sensitivity to the presence of a particle is restricted to distances of about $\alpha^{-1} \approx 1$ cm, we assume for simplicity that $\mathbf{r}'(\tau)$ evolves along the x axis from $-\infty$ to $+\infty$ at each rotation period (see Fig. 3). Using these assumptions and the approximation of the function $\delta u(\mathbf{r}, 0)$ by the series of Laguerre functions (see the Appendix) one can get the following expression for the dc normalized autocorrelation function [16]:

$$R_{\text{dc}}(\tau) = \frac{K_{\text{dc}}(\tau)}{K_{\text{dc}}(0)} = \frac{e^{-[d(\tau)]^2 \sigma / 4(1 + \sigma\tau D_x)} \operatorname{erf} \left(\frac{R-2\Delta}{\sqrt{D_z\tau}} \right)}{\sqrt{(1 + \sigma\tau D_x)(1 + \sigma\tau D_y)}}, \quad (18)$$

where $d(\tau)$ is the x component of the vector $\mathbf{r}'(\tau)$, which describes the regular periodic motion and $\sigma^{-1/2}$ is the characteristic decay length of the function $\delta u(\mathbf{r}, 0)$ along the x and y directions in the first order of the Laguerre function approximation [see Eq. (A2)], and $\text{erf}(s) = (2/\sqrt{\pi}) \int_0^s e^{-t^2} dt$ is the error function.

Since Eq. (12) gives the instantaneous phase fluctuation in terms of the sum over single-particle contributions [Eq. (13)] as is done for the dc, the correlation function for the phase

may be estimated using the general expression of the same form as Eq. (16) for the dc:

$$K_{\text{phase}}(\tau) = n \int \int \delta\phi(\mathbf{r}_1) \delta\phi(\mathbf{r}_2) W_{\tau}(\mathbf{r}_1 \rightarrow \mathbf{r}_2) d^3\mathbf{r}_1 d^3\mathbf{r}_2, \quad (19)$$

where W_{τ} was defined above. In the Appendix, using the first-order approximation of function $\phi(\mathbf{r})$ by the series of associated Laguerre functions, we show that the normalized autocorrelation function for the phase has the form

$$\begin{aligned} R_{\text{phase}}(\tau) = & e^{-[d(\tau)]^2 \beta / 4(1 + \beta \tau D_x)} \text{erf}\left(\frac{R - 2\Delta}{\sqrt{D_z \tau}}\right) [32 + \beta \tau (128D_x + 64D_y) + \beta^2 \tau^2 [d^4 + 12d^2 D_x + 204D_x^2 + 4d^2 D_y + 264D_x D_y \\ & + 44D_y^2] + \beta^3 \tau^3 [12d^2 D_x^2 + 152D_x^3 + 2d^4 D_y + 32d^2 D_x D_y + 432D_x^2 D_y + 4d^2 D_y^2 + 184D_x D_y^2] + \beta^4 \tau^4 [44D_x^4 \\ & + 28d^2 D_x^2 D_y + 328D_x^3 D_y + d^4 D_y^2 + 20d^2 D_x D_y^2 + 300D_x^2 D_y^2] + \beta^5 \tau^5 [96D_x^4 D_y + 16d^2 D_x^2 D_y^2 + 224D_x^3 D_y^2] \\ & + 64\beta^6 \tau^6 D_x^4 D_y^2] / [32(1 + \beta \tau D_x)^{9/2} (1 + \beta \tau D_y)^{5/2}], \quad (20) \end{aligned}$$

where $\beta^{-1/2}$ is the decay length for the function $\delta\phi(\mathbf{r})$ along the x and y directions [see Eq. (A5)].

To discuss Eqs. (18) and (20) let us first note that both formulas have the exponential factors identical apart from the replacement of β by σ in Eq. (20). These factors give the damped-pulse form (see Fig. 3) to the curves of autocorrelation functions, while the terms in the denominators provide the correlation decay for large τ . If one sets $d=0$ in Eqs. (18) and (20), the corresponding curves decay monotonically. The origin of the peaks in the autocorrelation function is the periodic component of the particle motion, while the decay is due to the random diffusion of particles. Note that τ enters the denominator of the exponent argument as a multiple of D_x , so that this diffusion constant is responsible for the broadening of successive correlation peaks. At small τ [$\ll (\beta D_{x,y})^{-1}, (\sigma D_{x,y})^{-1}$] the evolution of both the dc and phase curves is mostly affected by the exponential terms. Particularly, if one assumes a linear dependence of d on τ , these terms provide a Gaussian decay with the characteristic decay constants proportional to σ and β for the dc and phase autocorrelation functions, respectively. Typical values of σ that provide the best approximation of $\int_0^\infty \delta u^2(\psi, 0) d\psi$ (see the Appendix) with only the zero order term in Eq. (A2) are about 3.6 cm^{-2} , while the optimum values of β are somewhat less (about 3.3 cm^{-2}). In other words, when a particle recedes from the probe, the probe feels the particle in the phase longer than in the dc. This is why, according to Eqs. (18) and (20), the autocorrelation function for the phase decays slower than that for the dc. For large τ [$\gg (\beta D_{x,y})^{-1}, (\sigma D_{x,y})^{-1}$] one can neglect the unity in the denominators of the right-hand sides of both Eqs. (18) and (20). Also, all terms of order less than six in the numerator polynomial in Eq. (20) can be neglected. Consequently, at large τ both curves decay as τ^{-1} . The factor $\text{erf}[R - 2\Delta/\sqrt{D_z \tau}]$ in Eqs. (18) and (20) describes the correlation decay due to the diffusion along the z axis. This decay

is slower than those introduced by the exponential and denominator terms because of the probe weak sensitivity to particle displacement in the z direction. One should note that Eqs. (18) and (20) essentially represent the normalized autocorrelation functions of the dc and phase responses for a single-particle random perturbation. Their proportionality to the dc and phase correlation functions, where the coefficients linearly depend on the particle concentration, is the consequence of the assumption of the statistical independence of the motion of each particle from the others. For the phase correlation function the linear dependence on n is also a result of the approximation made to obtain Eq. (12) from Eq. (11).

IV. EXPERIMENTAL RESULTS

A. Fit of average values

Equations (9) and (15) derived in Sec. III may be compared with the frequency domain parameter time-averaged data obtained using the instrumentation described in Sec. II. For a discrete set of M source-detector distances R_i we obtained three data sets for the time-averaged dc and phase values $y_{i,j}$. These data sets correspond to measurements made at various (i) concentrations n_j of large particles with an effective radius $a=0.79 \text{ mm}$; (ii) concentrations n_j of small particles with an effective radius $a=0.50 \text{ mm}$; (iii) absorption coefficients μ_{aj} for the constant concentration $n=0.6 \text{ cm}^{-3}$ of small particles. The effective radius of the particles was estimated from the measurement of the volume occupied by a known large number (1800) of particles. The smaller particles were produced from the larger ones by cutting each into four pieces, so that the average radius ratio equals $4^{1/3}$. To vary the absorption coefficient of the medium we employed various concentrations of black India ink. The data were fitted by curves $Y_{a,q_j}(R)$ given by Eq. (9) for the dc or Eq. (15) for the phase. The parameter a was imposed to

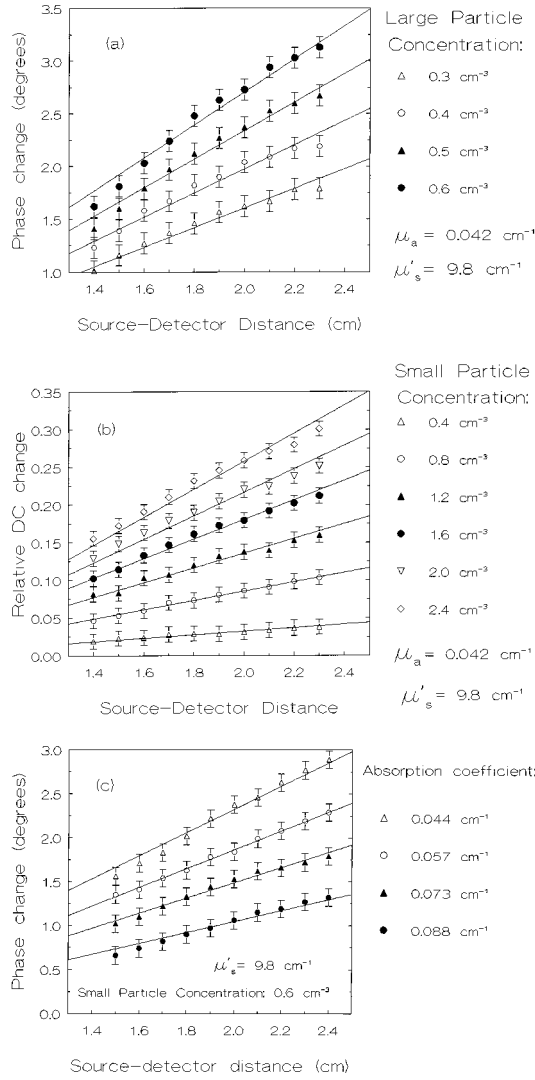


FIG. 5. (a) Average values of the phase change for different concentrations of large particles (0.79 mm effective radius); (b) average relative dc change for different concentrations of small particles (0.50 mm effective radius); (c) average phase change for different absorption coefficients of the turbid medium. The points represent the experimental data as a function of source-detector distance, while the lines are the best theoretical fits.

have the same value for a given data set and corresponds to the particle effective radius. N values q_1, \dots, q_N of the parameter q (where N is the number of curves in each data set) vary for different curves within each data set and correspond to n_j for the first and second data sets and to μ_{aj} for the third one. The fitting algorithm is based on the minimization of the χ^2 function [18],

$$\chi^2(a, q_1, \dots, q_N) = (NM - N - 1)^{-1} \times \sum_{j=1}^N \sum_{i=1}^M \frac{[y_{i,j} - Y_{a,q_j}(R_i)]^2}{\nu_{i,j}^2} \quad (21)$$

(where $\nu_{i,j}$ are the standard deviation errors in the measurements $y_{i,j}$) with respect to the values of the parameters a, q_1, \dots, q_N . The parameters providing the best fit are reported in Table I, while Figs. 5(a)–5(c) illustrate the good-

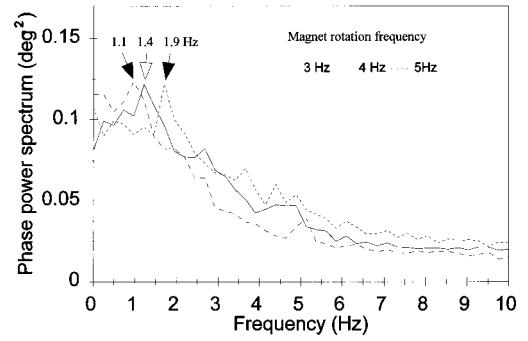


FIG. 6. Phase power spectra acquired at three successively increasing magnet rotation frequencies. The arrows indicate the frequencies corresponding to the peaks. The experimental conditions are the same as in Fig. 2, apart from the effective particle radius (0.50 mm).

ness of the fit. From Figs. 5(a)–5(c) and Table I one can see that Eqs. (9) and (15) fit the data with parameters that are in good agreement with the expected ones. A small negative curvature exhibited by the sets of data points may be related to the nonhomogeneity of the particle spatial distribution, which is larger near the beaker wall and smaller near its center. Since in our measurements the fiber nearest to the wall was fixed and the source-detector distance was changed by moving the other fiber towards the beaker center, the effective concentration of the particles was decreasing with distance. Note that while the fitted radii in the first two data sets are consistently smaller than the expected ones, the ratio of the large to small fitted radii is 1.7, close to the expected value of $4^{1/3} \approx 1.6$.

B. Fit of power spectra

Figure 6 shows the experimental power spectra of the phase fluctuations obtained for three different mixing magnet rotation rates. One can see that each curve has a maximum peak at a frequency that increases with the magnet rotation rate. There are also peaks at the harmonics of these frequencies. This confirms that the particle motion may be considered as the superposition of the periodic and random components assumed for the derivation of Eqs. (18) and (20). The fact that the maximum peak frequency for each curve in Fig. 6 is more than two times smaller than the corresponding frequency of the magnet rotation is explained by the spiral-like character of particle motion, such that particles return to the probe after traveling along a number of vertically stretched loops.

Another assumption used to obtain the dc and phase autocorrelation functions is the statistical independence of the particle motion. To check its validity, power spectra were obtained for different concentrations of particles. From Fig. 7(a) one can see that most of the spectrum increases homogeneously with concentration and approximately doubles when the concentration doubles, in agreement with the assumption made. To check this point quantitatively we plot the integral of the dc power spectrum as a function of particle concentration [Fig. 7(b)]. Figure 7(b) shows that the integrated dc power spectrum increases somewhat faster than linearly, and the divergence from a straight line becomes more significant at large concentrations (note that the inset,

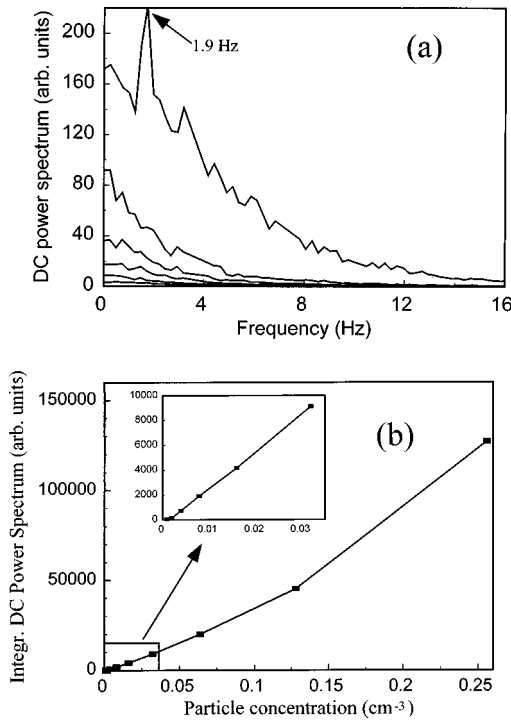


FIG. 7. (a) dc power spectra for different particle concentrations. From bottom to top, the curves correspond to particle concentrations of 0.008, 0.016, 0.032, 0.064, 0.128, and 0.256 cm^{-3} . (b) Integrated dc power spectrum vs particle concentration. The inset shows an enlarged view of the boxed part of the curve in the main plot.

corresponding to very small particle concentrations, shows an almost perfect linearity). The curve deviation from the linearity may be related to the power spectrum peak at the average particle rotation frequency, which increases faster than the rest of the spectrum and becomes more pronounced at large concentrations [Fig. 7(a)]. One can attribute this fast growth of the resonant peak to the correlations among particles, which are not included in the theoretical model.

The real picture of particle motion may be more complicated than the one assumed in our theoretical model, and its detailed investigation is beyond the goals of the present paper. However, some of the correlation function characteristics predicted by the model are observed experimentally. Figure 3 shows the normalized autocorrelation functions for the dc and phase obtained from the power spectra by means of the inverse discrete Fourier transform. The behavior of these curves is in qualitative agreement with the theoretical results: (i) both curves exhibit damped pulsations with a period comparable to that of the mixer rotation rate, and (ii) the dc autocorrelation decays faster than that of the phase. To verify experimentally Eqs. (18) and (20), we fitted the experimental power spectra to the theoretical curves by adjusting the values of the diffusion constants D_x, D_y, D_z . Figure 8 shows fits for the dc and phase spectra, where the theoretical curves are obtained from the discrete Fourier transform of the autocorrelation functions given by Eqs. (18) and (20). The function $d(\tau)$ in Eqs. (18) and (20), representing the regular periodic component of particle motion, is simulated by the function $L \tan(\pi\tau\Omega)$, where $L=4$ cm is the radius of a horizontal circle centered at the beaker vertical axis and

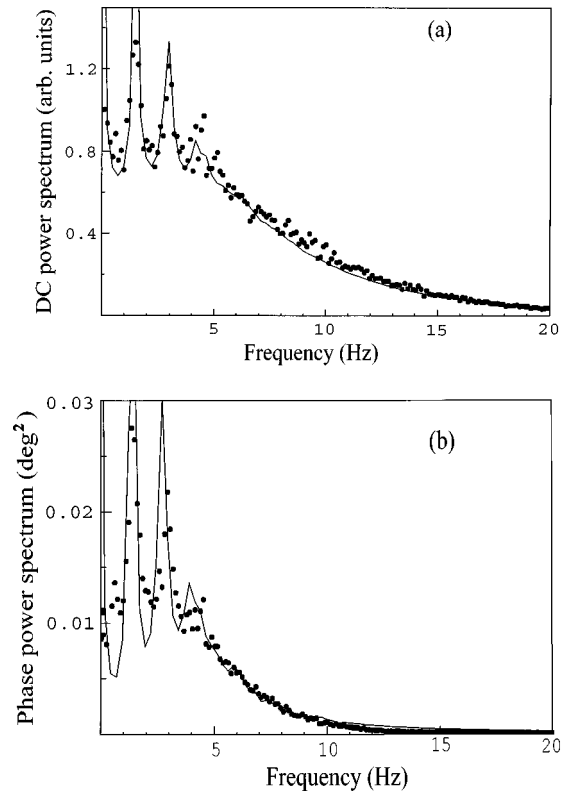


FIG. 8. The dc (a) and phase (b) power spectra. The points represent the experimental data, while the lines are the best fits provided by Eq. (18) [panel (a)] and Eq. (20) [panel (b)]. The data are obtained in the following experimental conditions: particle effective radius and concentration are, respectively, 0.5 mm and 0.3 cm^{-3} , magnet rotation frequency is 4 Hz. In the theoretical curves the effective particle rotation frequency is 1.5 Hz. Although the frequency band investigated extends up to 62.5 Hz, the frequency axis is limited to 20 Hz because the particle motion does not contribute to the power spectrum at larger frequencies.

passing through the middle of the line joining the source and detector fibers (Fig. 4), and Ω is the rotation rate. Such a choice of $d(\tau)$ provides a kind of motion in which the particle periodically recedes to infinity and returns back to the probe. To obtain the theoretical curves shown by the continuous lines in Fig. 8, all the parameters entering Eqs. (18) and (20) (apart from the diffusion constants) are set equal to their experimental values. The diffusion constant values providing the best fit are $D_x = D_y = D_z = 6$ cm^2/s . One can see that the theoretical curves are in good quantitative agreement with the experimental data.

V. DISCUSSION AND CONCLUSION

Data acquired with a sampling rate of 125 Hz show that our instrument is appropriate to investigate optical fluctuations in the frequency band of 0–62.5 Hz (processes on a time scale of 16 msec or slower), and over a spatial size as small as 1 mm. Reference [7] has presented measurements of temporal changes in the human occipital cortex optical parameters during visual stimulation. Since the characteristic time of the observed process is about 100 ms, the authors assign their observation to the neuronal activity. As reported by Gratton *et al.* [7], optical signals corresponding to specific

brain functions are very weak, having amplitude comparable to that of the underlying noise due to biological activity and the instrument noise. The instrument noise is statistically independent of the specific process under study and subtracting its spectrum from the power spectrum of the process can filter it out. Following this approach, we performed a measurement to obtain the dc and phase fluctuation power spectra using only one cross-correlation period per data point. The minimum period corresponded to a time resolution of 0.2 ms and a maximum sampling frequency of 5 kHz. In our test we collected data for the same total amount of time, but using different sampling rates. These power spectra and those obtained at a sampling interval of 8 ms essentially coincide in the frequency band 0–62.5 Hz. This test demonstrates that the maximum effective sampling rate of our instrument extends up to 5 kHz.

Theoretical calculations confirmed by measurements reveal that both phase and dc power spectra are proportional to the concentration of particles and to the fourth power of their effective radius. For particles having an effective diameter of 1 mm at a concentration of 0.3 cm^{-3} we measured a signal-to-noise ratio (SNR) of 22 dB for the phase power spectrum at the maximum peak frequency. Using the above theoretical result to scale this value, we found that the phase SNR becomes 0 dB for particles with an effective diameter of 0.6 mm at a concentration of 0.3 cm^{-3} . Alternatively, it decreases to 0 dB for particles with an effective diameter of 1 mm and at a concentration of 0.03 cm^{-3} . The dc SNR's are typically much higher. For the same conditions at which the phase power spectrum SNR is 22 dB, the dc maximum peak SNR is 41 dB. These results give an indication of what is the smallest measurable size of particles at a given concentration (and in our experimental conditions).

Our measurements show that the phase and the dc of photon-density waves propagating through a turbid medium with fluctuating optical properties have quantitatively different statistical properties. Namely, the phase correlation function decays slower than that of the dc. This effect reflects the well-established property of the dc and phase signals to explore different spatial regions. The dc signal is very sensitive to the region close to the source and detector fibers. Instead the phase signal responds more uniformly to the region between the source and the detector.

The statistical model we have used to describe the particle motion corresponds to the so-called model of homogeneous stationary turbulence [17]. We realize that this model is very rough and does not include many features of the real particle motion. However, the goal of the present work is not the investigation of the properties of the particle motion in the flow, but the demonstration of the method to study fluctuations of the optical parameters in turbid media. The values of the particle diffusion constants (about $6 \text{ cm}^2/\text{s}$) obtained from the experimental power spectra are consistent with the observed average speed of particles (about 5–10 cm/s), which confirms the validity of the method.

We note that although the system we have studied is far from being a perfect model of any real tissue, some of its features are similar to those observed in tissues [7]. For instance, the occurrence of areas having optical properties differing from those of the background medium, the temporal fluctuations in the local optical properties, and the presence

of a periodic component in the process (provided in tissues by the heart beat).

In conclusion, using the diffusion approximation for light transport in turbid media we have obtained analytical expressions for the mean changes in the dc and phase due to the motion of absorbing particles. Our measurements show that these expressions are in good agreement with the experimental data. In our case, the measurement of macroscopic fluctuation of optical parameters in turbid media provides information about the underlying physical processes and their time characteristics.

The results and methods presented in this work may be used to develop a high temporal resolution technique for the study of functional processes related to blood flow and oxygenation, and to neuronal activity.

ACKNOWLEDGMENT

This work was supported by NIH Grant Nos. RR03155 and CA57032.

APPENDIX

To perform the integration in Eq. (16) we replace the function $\delta u(\mathbf{r},0)$ by a suitable approximation. Due to the axial symmetry, this function depends only on two spatial coordinates, which may be chosen as the distance ρ from the particle to the source-detector line (see Fig. 4) and the longitudinal coordinate z along this line. Using Eq. (4) one can check that the change in $\delta u(\mathbf{r},0) = \delta u(\rho,z,0)$ with z is only significant in the vicinity of the source or the detector. Since the source and detector are confined by the tubes, we let $z = R/2$, so that Eq. (4) becomes

$$\delta u(\rho, R/2, 0) \approx \frac{A_\omega}{4\pi} \frac{\exp[-2\alpha\sqrt{(R/2)^2 + \rho^2}]}{(R/2)^2 + \rho^2}. \quad (\text{A1})$$

The next step is to approximate Eq. (A1) by the weighted series of N Laguerre polynomials $L_n(\sigma\psi)$ [19]:

$$\frac{A_\omega}{4\pi} \left(\sum_{n=1}^N h_n L_n(\sigma\psi) \right) \exp(-\sigma\psi/2), \quad (\text{A2})$$

where $\psi = \rho^2$ and

$$h_n = \sigma \int_0^\infty \frac{\exp[-2\alpha\sqrt{(R/2)^2 + \psi} - \sigma\psi/2]}{(R/2)^2 + \psi} L_n(\sigma\psi) d\psi. \quad (\text{A3})$$

The substitution of Eq. (A1) with the series (A2) is advantageous to estimate the correlation function for the following reasons. First, one can vary the parameter σ , which specifies the “width” of the Laguerre functions, such that the first term in Eq. (A2) agrees with Eq. (A1) to within 10%. Second, in the limit of large τ the double integral in Eq. (16) turns into the square of an integral of the form $\int_0^\infty \delta u(\psi,0) d\psi$. The approximation of a function by the series of weighted orthogonal polynomials provides the minimization of the error in the estimation of the integral of the function with respect to all possible polynomial approximations of the same order. Therefore, the series (A2) gives a good

approximation for the correlation function at large τ . In addition, the value of the parameter σ may be chosen to minimize not the error in the function approximation itself, but the error in the estimation of $\int_0^\infty \delta u^2(\psi, 0) d\psi$, which is the principal term entering the expression for the dc autocorrelation function at $\tau=0$. In this way the parameter σ naturally becomes dependent on the physical characteristics of the system, such as the source-detector distance R and the absorption and reduced scattering coefficients μ_a and μ_s' .

Keeping a large enough number of terms in Eq. (A2) one may calculate the correlation function to any desired accuracy. However, since we have no detailed information about the statistics of the particle motion, we can analyze the situation only qualitatively. For this reason we keep only the first term in the series (A2) to derive the expression for the dc autocorrelation function given by Eq. (18).

Like the function $\delta u(\mathbf{r}, 0)$, the single-particle contribution to the phase fluctuation $\delta\phi(\mathbf{r})$ given by Eq. (13) depends slowly on the longitudinal coordinate z and may be approximated as

$$\delta\phi(\rho) \approx R \frac{\text{Im}(A_\omega \exp\{2ik[\sqrt{(R/2)^2 + \psi} - R/2]\})}{(R/2)^2 + \psi}. \quad (\text{A4})$$

The next step for calculating the integral in Eq. (19) is the substitution of the right-hand side of Eq. (A4) by a weighted series of orthogonal polynomials. The only difference from the dc case is that a quicker convergence to the approximated function may be obtained using the set of associated Laguerre polynomials of the first order $L_n^1(\beta\psi)$, where β is the characteristic width of the function in the right-hand side of Eq. (A4). This function is approximated by the series

$$R \left(\sum_n g_n L_n^1(\beta\psi) \right) (\beta\psi) \exp(-\beta\psi/2), \quad (\text{A5})$$

where the coefficients are

$$g_n = \beta \Gamma(n+1) / [\Gamma(1+n+1)]^3 \int_0^\infty \frac{\text{Im}(A_\omega \exp\{2ik[\sqrt{(R/2)^2 + \psi} - R/2]\})}{(R/2)^2 + \psi} \exp(-\beta\psi/2) L_n^1(\beta\psi) d\psi, \quad (\text{A6})$$

and β is chosen to minimize the error in the calculation of the integral of $\delta\phi^2(x)$. Keeping only the first term in the series (A5), one obtains the autocorrelation function for the phase given in Eq. (20).

-
- [1] G. Maret and P. E. Wolf, *Z. Phys. B* **65**, 407 (1987).
 [2] M. Rosenbluh, M. Hoshen, I. Freund, and M. Kaven, *Phys. Rev. Lett.* **58**, 2754 (1987).
 [3] D. J. Pine, D. A. Weitz, P. M. Chaikin, and E. Herbolzheimer, *Phys. Rev. Lett.* **60**, 1134 (1988).
 [4] D. J. Pine, D. A. Weitz, J. X. Zhu, and E. Herbolzheimer, *J. Phys. (France)* **51**, 2101 (1990).
 [5] G. Gratton, M. Fabiani, D. Friedman, M. A. Franceschini, S. Fantini, P. Corballis, and E. Gratton, *J. Cogn. Neurosci.* **7**, 446 (1995).
 [6] R. Wenzel, H. Orbig, J. Ruben, K. Villringer, A. Thiel, J. Bernardin, U. Dirnagl, and A. Villringer, *J. Biomed. Opt.* **1**, 399 (1996).
 [7] G. Gratton, P. M. Corballis, E. Cho, M. Fabiani, and D. C. Hood, *Psychophysiology* **32**, 505 (1995).
 [8] A. Ishimaru, *Wave Propagation and Scattering in Random Media* (Academic, New York, 1978).
 [9] A. Ishimaru, *Appl. Opt.* **28**, 2210 (1989).
 [10] B. J. Tromberg, L. O. Svaasand, T.-T. Tsay, and R. C. Haskell, *Appl. Opt.* **32**, 607 (1993).
 [11] S. R. Arridge, M. Cope, and D. T. Delpy, *Phys. Med. Biol.* **37**, 1531 (1992).
 [12] B. A. Feddersen, D. W. Piston, and E. Gratton, *Rev. Sci. Instrum.* **60**, 2929 (1989).
 [13] S. Fantini, M. A. Franceschini, J. S. Maier, S. A. Walker, B. Barbieri, and E. Gratton, *Opt. Eng. (Bellingham)* **34**, 32 (1995).
 [14] S. Fantini, M. A. Franceschini, J. B. Fishkin, and E. Gratton, *Proc. SPIE* **2131**, 356 (1994).
 [15] D. A. Boas, M. A. O'Leary, B. Chance, and A. G. Yodh, *Proc. Natl. Acad. Sci. USA* **91**, 4887 (1994).
 [16] R. L. Stratonovich, *Topics in the Theory of Random Noise* (Gordon and Breach, New York, 1967).
 [17] M. W. Reeks, *Phys. Fluids A* **3**, 446 (1991).
 [18] P. R. Bevington and D. K. Robinson, *Data Reduction and Error Analysis for the Physical Sciences*, 2nd Ed. (McGraw-Hill, New York, 1992), p. 195.
 [19] G. Arfken, *Mathematical Methods for Physicists* (Academic Press, San Diego, 1985), p. 724.